# L-Type $Ca^{2+}$ Channels Access Multiple Open States to Produce Two Components of Bay K 8644–dependent Current in $GH_3$ Cells

DANIEL M. FASS* and EDWIN S. LEVITAN*‡

From the Departments of *Neuroscience and ‡Pharmacology, University of Pittsburgh, Pittsburgh, Pennsylvania 15261

ABSTRACT To determine the number of L-channel populations responsible for producing the two components of whole-cell L-type $Ca^{2+}$ channel current revealed by Bay K 8644 (Fass, D.M., and E.S. Levitan. 1996. *J. Gen. Physiol.* 108:1–11), L-type $Ca^{2+}$ channel activity was recorded in cell-attached patches. Ensemble tail currents from most (six out of nine) single-channel patches had double-exponential time courses, with time constants that were similar to whole-cell tail current decay values. Also, in single-channel patches subjected to two different levels of depolarization, ensemble tail currents exactly reproduced the voltage dependence of activation of the two whole-cell components: The slow component is activated at more negative potentials than the fast component. In addition, deactivation of Bay K 8644–modified whole-cell L-current was slower after long (100-ms) depolarizations than after short (20-ms) depolarizations, and this phenomenon was also evident in ensemble tail currents from single L-channels. Thus, a single population of L-channels can produce the two components of macroscopic L-current deactivation. To determine how individual L-channels produce multiple macroscopic tail current components, we constructed ensemble tail currents from traces that contained a single opening upon repolarization and no reopenings. These ensemble tails were biexponential. This type of analysis also revealed that reopenings do not contribute to the slowing of tail current deactivation after long depolarizations. Thus, individual L-channels must have access to several open states to produce multiple macroscopic current components. We also obtained evidence that access to these open states can vary over time. Use of several open states may give L-channels the flexibility to participate in many cell functions. Key words: calcium channel • dihydropyridine • single channel • pituitary

## INTRODUCTION

$Ca^{2+}$ influx through L-type voltage-gated $Ca^{2+}$ channels is the key event in the coupling of secretion, contraction, and gene expression to membrane excitation in many cell types (Hille, 1992; Murphy et al., 1991). L-currents, which are sensitive to dihydropyridine drugs, show heterogenous behaviors. In particular, L-current kinetics varies in different cell types (Hess, 1990; Tanabe et al., 1991), and multiple kinetic components of L-current are observed within single cells (Richard et al., 1990, 1993; Tiaho et al., 1994; Fass and Levitan, 1996). A key question is whether these multiple components of L-current arise from multiple populations of L-channels or from complex gating properties of a single population. In either case, it is likely that the diversity of L-current behaviors is necessary to support the multiple functional roles played by L-channels in various cell types.

In $GH_3$ rat clonal pituitary cells, L-channels are thought to play a key role in excitation–secretion coupling (Enyeart et al., 1985), stimulation of gene expression (Duchemin et al., 1992), triggering action potentials (Scherübel and Hescheler, 1991), and setting resting intracellular $Ca^{2+}$ levels (Mollard et al., 1994). Recent $GH_3$ cell mRNA analyses have revealed the expression of genes encoding both the $\alpha_{1C}$ and $\alpha_{1D}$ L-channel pore-forming subunits (Lievano et al., 1994). Thus, two genetically distinct populations of L-channels may exist in $GH_3$ cells. Direct studies of $GH_3$ L-channel activity by patch–clamp methods have revealed a diversity of behaviors. For example, multiple conductance levels (Kunze and Ritchie, 1990; Mantegazza et al., 1995) and two distinct opening probabilities and inactivation rates (Mantegazza et al., 1995) are evident. Whether these diverse behaviors arise from multiple populations of L-channels or from the complex gating properties of a single population has yet to be investigated. Moreover, the contribution of these diverse behaviors to the various roles L-channels play in $GH_3$ cells is also not known.

We have studied macroscopic L-type $Ca^{2+}$ channel currents in $GH_3$ cells. In the presence of the dihydropyridine agonist Bay K 8644, these L-currents exhibit a dramatically slowed tail current decay that consists of two distinct kinetic components (Fass and Levitan, 1996). We have characterized various properties of the two components. In particular, the two components differ in sensitivity to Bay K 8644, in the degree to which they are inhibited by thyrotropin-releasing hor-

Address correspondence to Edwin S. Levitan, E1355 Biomedical Science Tower, Department of Pharmacology, University of Pittsburgh, Pittsburgh, PA 15261. Fax: (412) 648-1945; E-mail: Levitan@bns.pitt.edu


J. GEN. PHYSIOL. © The Rockefeller University Press • 0022-1295/96/07/13/14 $2.00
Volume 108 July 1996 13–26

mone, and in voltage dependence of activation. Thus, Bay K 8644 reveals multiple components of macroscopic L-current in $GH_3$ cells.

In the present study, we have attempted to determine the single-channel basis for these two components. Specifically, we have tested whether they arise from one or multiple populations of L-channels. Our primary finding is that the averaged behaviors of single L-channels can form a quantitatively accurate reproduction of several of the most prominent features of macroscopic L-currents. This suggests that the complex gating properties of a single population of L-channels can create the two components of macroscopic L-current recorded in the presence of Bay K 8644 in $GH_3$ cells. Furthermore, we find that the two macroscopic components arise from multiple open states accessed by individual L-channels in this population. Access to several open states may give these channels flexibility to carry out several functional roles.

## MATERIALS AND METHODS

### *Cell Culture*

$GH_3$ cells were obtained from the American Type Culture Collection (Rockville, MD). The cells were grown at 37°C and 5% $CO_2$ in Ham's F-10 medium supplemented with 15% horse serum and 2.5% fetal calf serum. After passage, cells were plated in 35-mm culture dishes in the same medium and serum. Cells were used for electrophysiological experiments 1 to 6 d after passage.

### *Patch-Clamp Experiments*

Standard cell-attached and whole-cell patch-clamp methodology was used (Hamill et al., 1981). For cell-attached experiments, the bath solution contained the following (in mM): 150 KCl, 3 $MgCl_2$, 0.05 $K_3$-EGTA, 10 HEPES, and 20 glucose, pH 7.4. The pipette solution contained the following (in mM): 100 $BaCl_2$, 20 tetraethylammonium chloride (TEA·Cl), and 10 mM Na-HEPES, pH 7.4, along with 1 μM Bay K 8644. For whole-cell experiments, the bath solution contained the following (in mM): 150 NaCl, 0.8 $MgCl_2$, 5.4 KCl, 2 $CaCl_2 \cdot 2H_2O$, 20 glucose, 10 Na-HEPES, pH 7.4. After establishing the whole-cell configuration, a solution containing (in mM): 100 $BaCl_2$, 20 TEA·Cl, 10 Na-HEPES, pH 7.4, was superfused directly over the cell being studied. Superfusion was maintained continuously throughout all experiments. Whole-cell pipettes were filled with the following (in mM): 160 CsCl, 5 $MgCl_2$, 0.1 EGTA, 0.2 Na-GTP, 2.5 $Na_2$-ATP, 5 Cs-HEPES, pH 7.2, with NaOH. All solutions were filtered through 0.2-μm syringe filters (Gelman Sciences, Inc., Ann Arbor, MI).

Pipettes of 15–20-MΩ (cell-attached experiments) or 3.0–4.0-MΩ (whole-cell experiments) tip resistance were fabricated from Garner 7052 glass capillary tubes and coated with Sylgard (Dow Corning Corp., Indianapolis, IN). A patch clamp amplifier (Axopatch 200A; Axon Instruments, Inc., Foster City, CA) with an integrating head stage controlled by PCLAMP software (versions 6.0 and 6.0.1, Axon Instruments, Inc.) were used for data acquisition. Analog current signals were low-pass filtered at 2 or 5 kHz (cell-attached experiments) or 5 kHz (whole-cell experiments) and then digitized at 20 or 25 kHz (cell-attached experiments) or 20 kHz (whole-cell experiments). All traces have been leak subtracted by subtraction of averages of traces without openings (cell-attached experiments) or by a P/4 protocol (whole-cell experiments). For whole-cell experiments, series resistance was 5–9 MΩ after establishment of the whole-cell configuration, and was always compensated by 80%. All experiments were performed at room temperature (20–22°C).

In the figures, some traces have been digitally filtered at 3 kHz for presentation.

### *Identification of Openings in Single-Channel Patches*

The program Fetchan from the PCLAMP suite (version 6.0.1) was used to analyze single-channel records and to form idealized traces. Open and closed amplitudes were set manually. Single-channel openings were detected when the current amplitude rose above a threshold set at 50% of the open amplitude. Our criterion for the identification of a single-channel patch was the absence of overlapping openings in ≥200 traces.

### *Curve-fitting*

Fitting of exponentials to ensemble average tail currents or whole-cell tail currents was performed using the Clampfit program from the PCLAMP suite (versions 6.0 and 6.0.1). A simplex algorithm was used to find minimum sum-of-squared errors fits. Iterative fits converged when the simplex fractional error became <0.0001. In all fits, the first ~400 μs of the ensemble tail currents was ignored in the fitting procedure to avoid artifacts produced by the settling of the voltage clamp. Thus, amplitude values reflect the magnitude of ensemble tails at ~400 μs after repolarization.

Dwell-time histograms were plotted from idealized traces following the method of Sigworth and Sine (1987). Fitting of exponentials to these histograms was performed using the PSTAT program in the PCLAMP suite (version 6.0.1). A simplex algorithm was used to find maximum likelihood fits. To decide upon the number of exponential components (i.e., one or two) to use for an adequate fit of a given dwell-time histogram, we used a statistical test performed by PSTAT. This test involved calculating an F-statistic that evaluates whether the reduction in the sum-of-squared errors from the double-exponential fit (relative to the single-exponential fit) justifies the use of more free parameters.

Amplitude histograms were constructed from idealized traces. Fitting of Gaussians to these histograms was performed by PSTAT. A simplex algorithm was used to find minimum sum-of-squared errors fits. The number of Gaussians used to fit each histogram (i.e., one or two) was determined by eye.

### *Statistics*

Descriptive statistics were calculated by SYSTAT (version 5.02; Systat, Inc.). All values are given as mean ± SEM. Student's *t* tests were performed by SYSTAT or INSTAT (version 2.04a; GraphPAD Software for Science, San Diego, CA). A one-sample *t* test in INSTAT was used to compare groups of data with constants (as in Tables I, II, and IV).

### *Drugs*

A stock solution (5 mM) of Bay K 8644 was made in ethanol. The final concentration of ethanol was 0.02%. Bay K 8644 was generously donated by A. Scriabine (Miles Inc., West Haven, CT).

## RESULTS

### *Conductance of $GH_3$ L-Channels*

The most commonly observed conductance level for L-channels studied with high concentrations (~100

mM) of $Ba^{2+}$ as a charge carrier (McDonald et al., 1994) is ~25 pS. A study in $GH_3$ cells identified ~24-pS openings and also three lower conductance levels for L-channels (Kunze and Ritchie, 1990). We also observed multiple conductance levels. Using 100 mM $Ba^{2+}$ and 1 μM Bay K 8644, we observed large amplitude openings of ~2 pA at −50 mV, as well as very low amplitude openings (~0.5 pA). Amplitude histograms sometimes also had minor "shoulders," which presumably arise from medium amplitude openings (Fig. 1 *B*). Fig. 1 *A* shows representative traces from a single L-channel recorded during 100-ms depolarizations to −10 mV. Large amplitude openings are predominant in these and most of our data. From seven patches in which openings were recorded at three or more voltages, the conductance of the predominant large amplitude openings was 23.8 ± 0.4 pS (Fig. 1 *C*). L-channels with these ~24-pS openings are likely the same as the ~23 pS L-channels found in $GH_3$ cells (Levitan and Kramer, 1990) to be sensitive to inhibition by thyrotropin-releasing hormone.

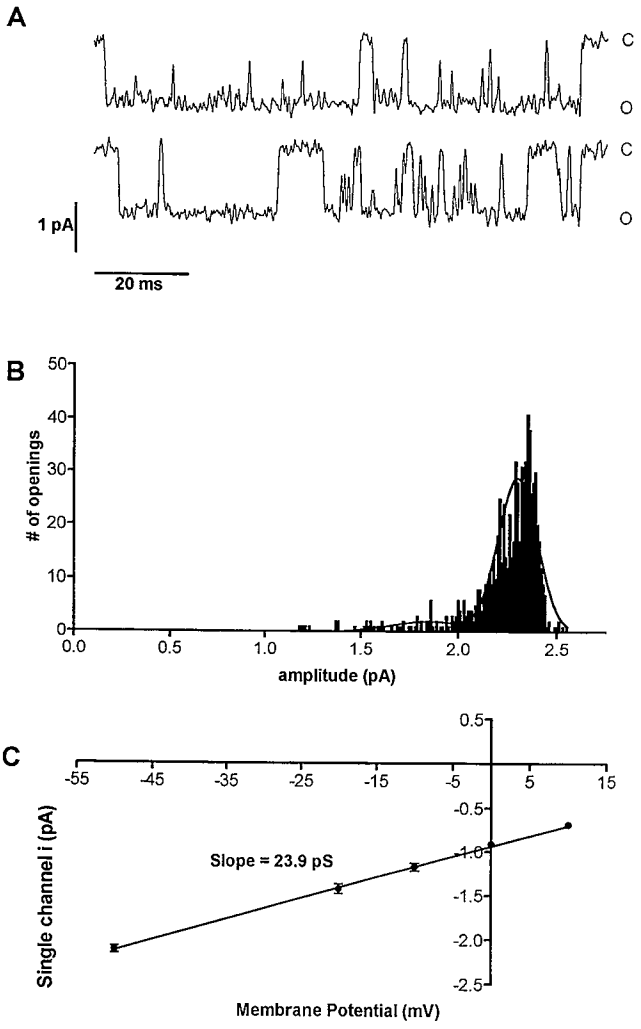


FIGURE 1. $Ba^{2+}$ conductance of L-channels in $GH_3$ cells. (*A*) Examples of openings of a single L-channel recorded during 100-ms depolarizations to −10 mV. *C*, baseline; *O*, open channel. (*B*) An example of an amplitude histogram from a single L-channel constructed from openings recorded at −50 mV. Note that the amplitude data contain one major component plus a minor low amplitude component. A double Gaussian fit is superimposed over the data. (*C*) A plot of single-channel amplitude vs voltage constructed using data from seven single-channel patches from which openings were recorded at three or more voltages. Amplitude values are from the major component of Gaussian fits of amplitude histograms. Each data point is the mean ± SEM of three to seven amplitude values.

In single-channel patches with ~24-pS openings, the very low amplitude openings were extremely rare or completely absent. However, we were occasionally able to record from patches containing only the very low amplitude openings. Therefore, it is likely that these very low amplitude openings arise from a different, rarer type of channel in $GH_3$ cells. The medium amplitude openings that give rise to the shoulders in some of our amplitude histograms may represent subconductance states of L-channels like those identified by Kunze and Ritchie (1990). If so, these subconductance states are visited infrequently (as indicated by the small size of the shoulders relative to the major peaks in amplitude histograms). Thus, we chose to focus our study on the ~24-pS openings.

### *Deactivation Kinetics of Single L-Channels Derived from Ensemble Average Tail Currents*

Initially, we wished to test whether L-channel activity in our cell-attached patch conditions was similar to the activity we had previously observed under whole-cell conditions (Fass and Levitan, 1996). Therefore, we recorded large numbers of traces from patches which contained two or more ~24-pS L-channels (multichannel patches). We used a depolarizing stimulus that was identical in amplitude and duration (+50 mV for 10 ms) to one used in our whole-cell study, and deactivation was monitored at −50 mV. Then, traces with events in the tail portion were used to construct ensemble average tail currents. Values for time constants and amplitudes taken from exponential fits of these ensemble average tail currents were then compared with constants taken from our whole-cell study. Since whole-cell tail currents were not recorded at −50 mV, approximate time constant and amplitude values for whole-cell tail current decay at −50 mV were obtained by averaging the mean values derived from exponential fits of tails at −40 and −60 mV (see Table I legend for these values). Fig. 2 shows representative individual sweeps and the ensemble average trace (with overlaid double-exponential tail fit) from a multichannel patch. The ensemble average tail current is fit by two exponentials with time constants similar to whole-cell values. From a total of eight patches, fits of ensemble averages showed that six

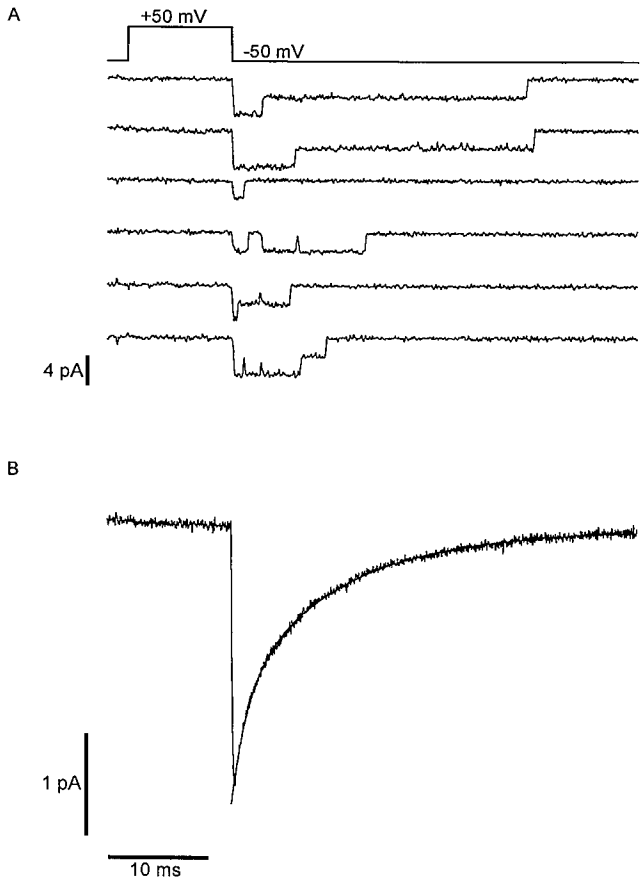


FIGURE 2. Ensemble average tail currents: multichannel patches. (Data in *A* and *B* are from the same patch). (*A*) Individual traces taken from a multichannel patch subjected to depolarization given every 2 s. Openings are visible only after repolarization to −50 mV (since the driving force for inward current is very small at +50 mV). The time scale is shown in *B*. (*B*) The ensemble average current constructed from 1,059 traces. A computer-generated double-exponential fit (*smooth curve*) is superimposed on the tail portion of the trace.

had double-exponential tails, one had a single-exponential tail with a decay rate similar to the whole-cell fast component, and one had a single exponential tail with a decay rate similar to the whole-cell slow component. Table I shows the data from exponential curve fits of all of our multichannel patches. The average values for $\tau_{fast}$ and $\tau_{slow}$ are not significantly different from whole-cell values ($P > 0.05$ in both cases). The average values for percent contribution to the total tail current are somewhat different from whole-cell values ($P = 0.03$ in both cases). This result appears to stem primarily from two patches (denoted by asterisks in Table I) that exhibited values of percent contribution that were reversed from the whole-cell case. To an approximation, these data suggest that L-channels in $GH_3$ cells behave similarly under our whole-cell and cell-attached conditions.

We also obtained data from nine single-channel patches. Fig. 3 shows representative traces and ensemble averages (with overlaid exponential tail fits) from two single-channel patches, and Table II shows the data obtained from all of our single-channel patches. Trends in the single-channel patch data were similar to those seen in the multichannel patch data. Fits of ensemble average tails showed that six L-channels had double-exponential tails, and three L-channels had single-exponential tails with decay rates similar to the

TABLE I

*Multichannel Patches: Summary of Exponential Fits of Ensemble Average Tail Currents*

| Patch | No. of channels | $\tau_{fast}$ | $\tau_{slow}$ | Percent fast | Percent slow |
|---|---|---|---|---|---|
| | | *ms* | *ms* | | |
| 401104 | ≥2 | 1.4 | 5.9 | 43 | 57 |
| 49080 | ≥3 | 1.6 | 5.0 | 48 | 52 |
| 4O050 | ≥3 | 0.6 | 9.6 | 57 | 43 |
| 4O103 | ≥6 | 2.1 | 8.1 | 68 | 32 |
| 491309* | ≥2 | 0.7 | 6.6 | 14 | 86 |
| 492004* | ≥2 | 1.6 | 10.3 | 35 | 65 |
| mean ± SEM | | 1.3 ± 0.2 | 7.6 ± 0.9 | 44.2 ± 7.6 | 55.8 ± 7.6 |

| Patch | No. of channels | $\tau$ |
|---|---|---|
| | | *ms* |
| 4921312 | ≥2 | 1.4 |
| 491401 | ≥2 | 9.0 |

(*Top*) Ensemble average tail currents fit by two exponentials ($n = 6$); (*bottom*) ensemble average tail currents fit by one exponential ($n = 2$). No. of channels is the observed maximum number of simultaneous openings. Hence, the numbers represent the minimum number of channels in each patch. Average $\tau$ and amplitude values taken from our whole-cell study (Fass and Levitan, 1996) for statistical comparison with means in this table were as follows: $\tau_{fast}$ = 1.5 ms, $\tau_{slow}$ 6 ms, $Percent_{fast}$ = 67.5, $Percent_{slow}$ = 32.5. *See Results concerning these two patches.

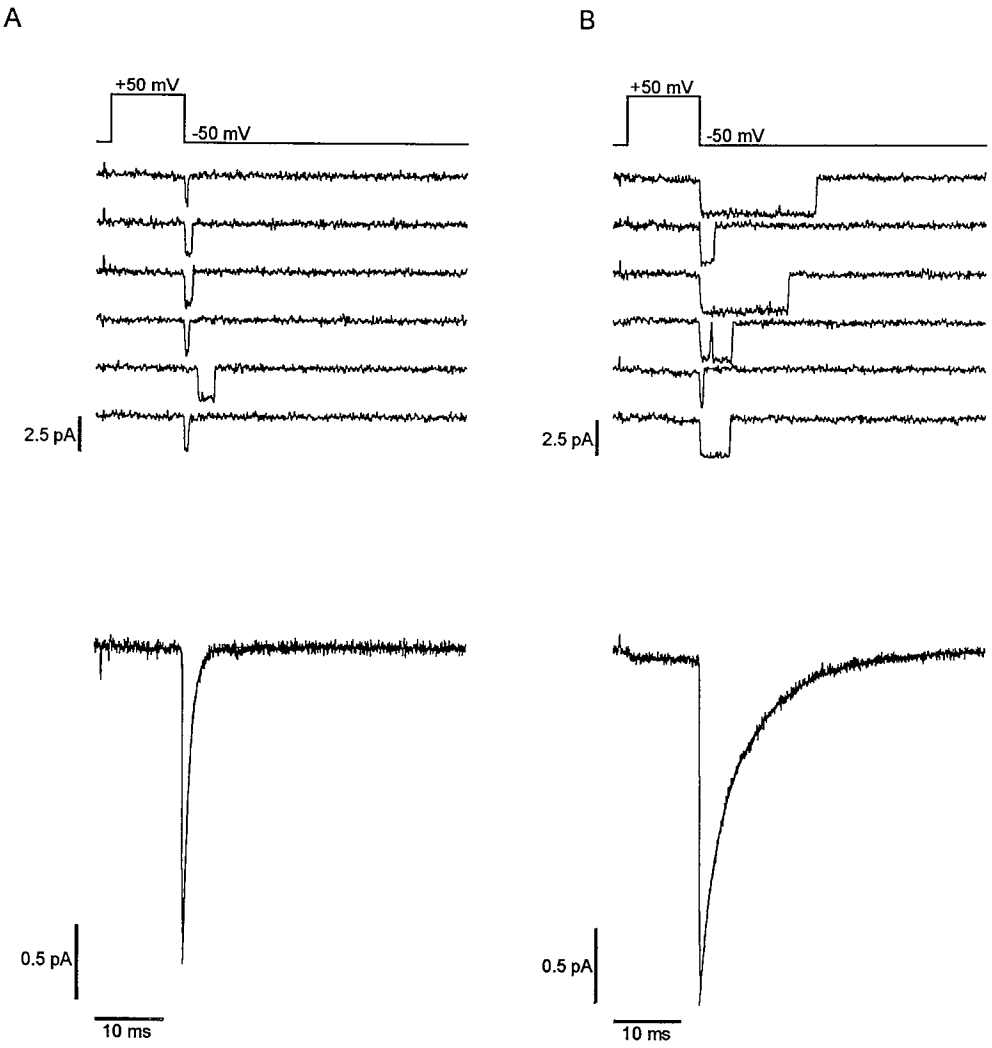


FIGURE 3. Ensemble average tail currents from two single-channel patches. Depolarizations were given every 2 s. The time scales are shown in the lower panels. Upper panels show individual traces, and lower panels show the ensemble average current constructed from 209 traces (*A*) and 796 traces (*B*). Computer-generated fits (single-exponential smooth curve in *A*; double-exponential smooth curve in *B*) are superimposed on the tail portions of the traces.

TABLE II

*Single-Channel Patches: Summary of Exponential Fits of Ensemble Average Tail Currents*

| Patch | $\tau_{fast}$ | $\tau_{slow}$ | Percent fast | Percent slow |
|---|---|---|---|---|
| | *ms* | *ms* | | |
| 4O10612 | 1.8 | 6.4 | 42 | 58 |
| 4O1304 | 1.8 | 5.1 | 62 | 38 |
| 4O0403 | 1.5 | 6.0 | 53 | 47 |
| 492102 | 2.6 | 9.8 | 79 | 21 |
| 4D2804 | 1.9 | 10.8 | 19 | 81 |
| 4O05713 | 1.7 | 7.2 | 32 | 68 |
| mean ± SEM | 1.9 ± 0.2 | 7.6 ± 0.9 | 48 ± 9 | 52 ± 9 |
| Patch | $\tau$ | | | |
| | *ms* | | | |
| 4O0535 | 1.7 | | | |
| 490103 | 0.9 | | | |
| 4914515 | 0.7 | | | |

(*Top*) Ensemble average tail currents fit by two exponentials ($n$ = 6); (*bottom*) ensemble average tail currents fit by one exponential ($n$ = 3).

whole-cell fast component. From the six patches with double-exponential ensemble average tails, the average values for the parameters $\tau_{fast}$, $\tau_{slow}$, and percent contribution of each component to the total ensemble average tail current were not significantly different from whole-cell values ($P > 0.05$ in all cases). The fact that single L-channels can produce double-exponential ensemble average tail currents, with time constants and amplitudes that are similar whole-cell tail current decay values, indicates that a single population of L-channels can produce both components of macroscopic tail current decay.

### *Multiple Open States Accessed during Bay K 8644–modified Deactivation*

Individual traces contained openings that were evident immediately upon repolarization (i.e., reflecting L-channels that were open when the membrane was repolarized), as well as openings that occurred after repolarization (i.e., "reopenings" reflecting L-channels that opened after the membrane was repolarized). These

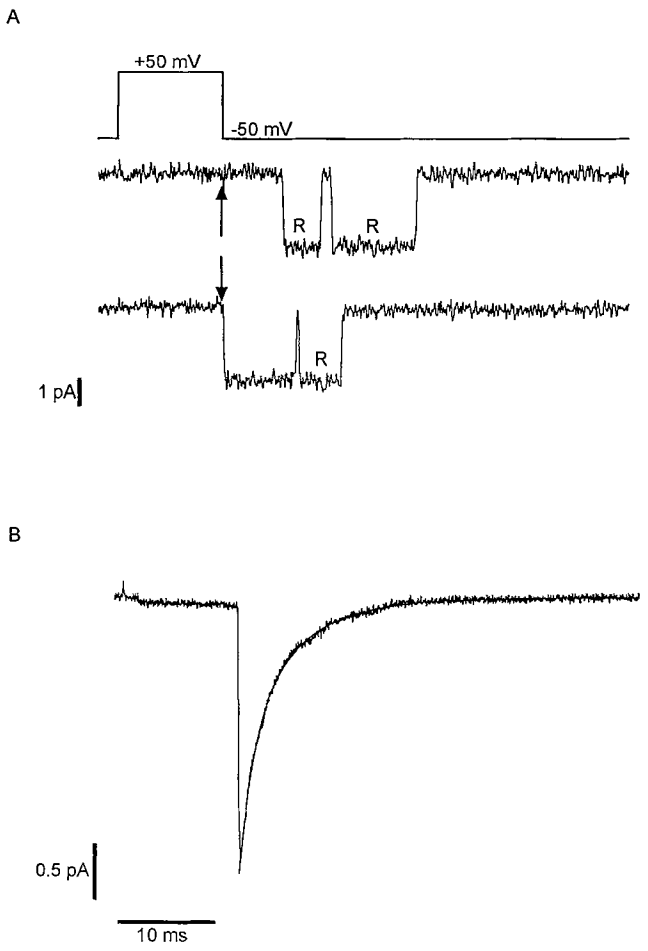


FIGURE 4. Reopenings of L-channels after repolarization. (*A*) Individual traces that illustrate two types of reopenings. The depolarization protocol is illustrated above the traces. Arrows pointing to current traces indicate the time of repolarization to −50 mV. Reopenings are designated with *R*. The upper trace illustrates the case of an L-channel that was not open upon repolarization, but opened twice within the 40 ms after repolarization. The lower trace illustrates the case of an L-channel that was open upon repolarization and reopened once after a brief closure within the 40 ms after repolarization. The time scale is shown in *B*. (*B*) Ensemble average current for a single-channel patch constructed from only those traces that contain no reopenings. A computer-generated double-exponential fit (*smooth curve*) is superimposed over the tail portion of the trace.

reopenings, which were present in every patch, sometimes occurred even when no opening was evident upon repolarization but occured more frequently when an L-channel that was open at repolarization closed briefly and then opened again. These two types of reopenings are shown in the two traces in Fig. 4 *A*.

To determine the number of open states that were accessed by each L-channel during deactivation, we formed ensemble average tail currents from only those traces that contained a single opening that was apparent upon repolarization. The number of exponentials required to fit the resulting "reopening-free" ensemble average tail current reflects the number of open states accessed by each L-channel during deactivation. These reopening-free ensemble average tail currents (Fig. 4 *B*) were constructed for all six single-channel patches that yielded a double-exponential ensemble average tail current when all traces were included (data are summarized in Table III). In all six cases, two exponentials were required to fit the reopening-free ensemble averages (mean $\tau_{fast}$ = ~1 ms, mean $\tau_{slow}$ = ~5 ms). This indicates the presence of two open states in the gating scheme of Bay K 8644–modified $GH_3$ cell L-channels.

Reopenings, if frequent, would contribute significantly to the time course of L-current deactivation. To examine the frequency with which reopenings occurred, we scored all tail traces for whether or not they contained a reopening. In the plots of Fig. 5, which show the chronological history of opening durations during deactivation for single L-channels, a tick above each data point (at 20 ms on the *y*-axis) indicates a tail trace in which a reopening occurred. Reopenings were more frequently observed in single-channel patches displaying biexponential deactivation than in single-channel patches displaying monoexponential fast component deactivation (compare Fig. 5 *A* with *B*). To quantitate the contribution of these reopenings to the time course of tail current decay, we compared parameters from exponential fits of the reopening-free ensemble average tail currents with parameters from ensemble average tail current formed with all traces included (Table III). The average values for $\tau_{fast}$ and $\tau_{slow}$ were smaller ($P < 0.01$ for both) in ensemble average tail currents constructed from only those traces that contained no reopenings. However, percent contribution of each exponential component to the total tail current was not different ($P > 0.05$). Thus, we conclude that reopenings contribute to both components of macroscopic tail current decay, each of which derives from a distinct open state.

### *Gating Patterns over Time*

Hypothetically, a single channel capable of accessing multiple open states may have continuous access to all possible open states, or, alternatively, the channel may experience distinct periods of activity in which gating is limited to a subset of the possible open states. We were able to record from patches containing single L-channels for up to 70 min. Therefore, we examined the gating behavior of L-channels across time. For this analysis, we measured the time to first closure for channels that were open upon repolarization (i.e., the dwell time of the first opening in the tail, excluding first openings that occurred after the time of repolarization). The score of 0 was given to traces in which no opening was

TABLE III

*Contribution of Reopenings to Deactivation: Comparison of Ensemble Average Tail Currents Constructed from All Traces To Reopening-free Ensemble Average Tails*

| Patch | All traces (same data as in Table II) | | | | Only traces without reopenings | | | |
|---|---|---|---|---|---|---|---|---|
| | $\tau_{fast}$ | $\tau_{slow}$ | Percent fast | Percent slow | $\tau_{fast}$ | $\tau_{slow}$ | Percent fast | Percent slow |
| | *ms* | *ms* | | | *ms* | *ms* | | |
| 4O0403 | 1.5 | 6.0 | 53 | 47 | 1.1 | 4.1 | 67 | 33 |
| 4O05713 | 1.7 | 7.2 | 32 | 68 | 1.4 | 5.3 | 44 | 56 |
| 4O10612 | 1.8 | 6.4 | 42 | 58 | 1.1 | 4.3 | 70 | 30 |
| 492102 | 2.6 | 9.8 | 79 | 21 | 1.7 | 8.0 | 82 | 18 |
| 4O1304 | 1.8 | 5.1 | 62 | 38 | 0.9 | 2.7 | 57 | 43 |
| 4D2804 | 1.9 | 10.8 | 19 | 81 | 0.9 | 5.2 | 11 | 89 |
| mean | 1.9 | 7.6 | 48 | 52 | 1.2 | 4.9 | 55 | 45 |
| ±SEM | 0.2 | 0.9 | 8.8 | 8.8 | 0.1 | 0.7 | 10.3 | 10.3 |

observed upon repolarization. We constructed graphs of L-channel gating behavior over time by plotting, in chronological order, the dwell-time score for each trace recorded from a given single-channel patch.

Fig. 5 shows L-channel gating behavior over time in four single-channel patches. Fig. 5, *A* and *B*, gives examples of single L-channels that showed no obvious changes in gating patterns over the course of the recording session. The L-channel in Fig. 5 *A* yielded a double-exponential ensemble average tail current in which the percent contributions to total for the fast and slow components were similar to whole-cell values. In this and the four other single-channel patches that yielded double-exponential ensemble average tail currents, short and long open times appeared intermingled. Fig. 5 *B* shows data from a single L-channel that yielded a single-exponential ensemble average tail current with a time constant similar to the fast whole-cell component. From this channel, openings evident upon repolarization were distributed sparsely across time. Very long openings (which are obvious in Fig. 5 *A*) are absent, even from the other 579 traces sampled from

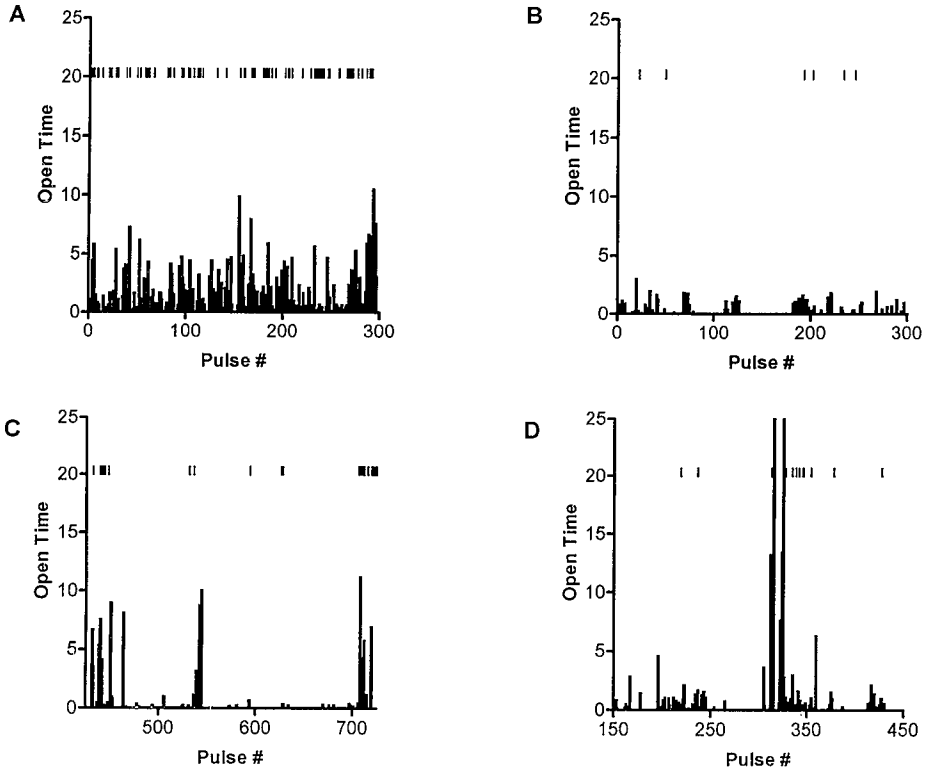


FIGURE 5. Tail event durations over time. The duration of the first event in each tail trace (excluding reopenings) or 0 (for tail traces with no openings or only reopenings) is plotted for each of 300 pulses given to a single-channel patch in chronological order. A vertical line segment at 20 on the *y*-axis is plotted for each trace that contained a reopening (of any duration). *A–D* represent data from four different single-channel patches.

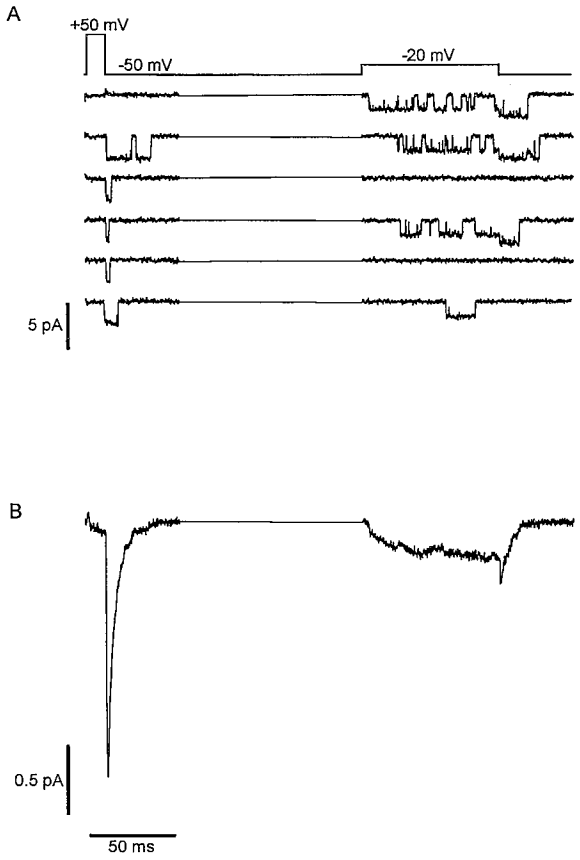


FIGURE 6. Ensemble average tail currents after two levels of depolarization. (*A*) Individual traces from a single-channel patch subjected to depolarizations every 3 s. The middle portions of the traces (100 ms at −50 mV) have been removed. The time scale is shown in *B*. (*B*) The ensemble average current trace constructed from 293 traces.

this channel. In total, seven of nine single L-channels showed no obvious changes in gating patterns over time. These L-channels seemed to have invariant access to either only one or both of the two open states.

Fig. 5, *C* and *D*, gives examples of single L-channels that showed changes in gating patterns over the course of the experiment. The channel in Fig. 5 *C* yielded a double-exponential ensemble average tail current in which the percent contribution of the slow component to the total tail current was larger than for the fast component (i.e., reversed from the whole-cell case). This L-channel exhibited very long openings at the beginning, at one point near the middle, and at the end of this series of traces. Most openings before and after this series were long. However, the plot illustrates that, for a period of time, this L-channel exhibited only sparse, short openings upon repolarization. There were too few openings during this time to construct an ensemble average tail current suitable for curve-fitting for a comparison of the time constant to the fast component time constant. However, it appears likely that this L-channel made a brief sojourn into a gating pattern similar to that seen for the L-channel in Fig. 5 *B* (i.e., fast component gating). Fig. 5 *D* shows data from a single L-channel that yielded a single-exponential ensemble average tail current with a time constant similar to the whole-cell fast component. As for the channel shown in Fig. 5 *B*, most openings evident upon repolarization from this channel were sparse and short. However, the plot illustrates that, for a brief period of time, the channel exhibited very long openings. As was the case for the L-channel in Fig. 5 *C*, there were too few openings during this time to construct an ensemble average tail current suitable for curve-fitting for a comparison of the time constant to the slow component time constant. However, it appears likely that this L-channel made a brief sojourn into a gating pattern characterized by very long openings (i.e., slow component gating). In total, two of nine single L-channels showed obvious changes in gating patterns over the course of the recording session. For these two L-channels, access to the two open states varied over time. A population made up of L-channels with varied access to the two open states can account for biexponential macroscopic tail current decay. Thus, it is not necessary to invoke separate populations of physically distinct (i.e., in subunit composition) L-channels to account for the single- and double-exponential ensemble average tail currents summarized in Table II. Rather, a single population of L-channels may account for all of our observations.

### *The Two Open States Have Different Voltage Dependences of Activation*

The two Bay K 8644–revealed components of whole-cell L-current have different voltage dependences of activation (Fass and Levitan, 1996): The slow component

TABLE IV

*Voltage Dependence of Access to the Two Open States: Summary of Exponential Fits of Ensemble Average Tail Currents Recorded at −50 mV after Depolarizations to +50 and −20 mV*

| | +50 mV | | | | −20 mV | |
|---|---|---|---|---|---|---|
| Patch | $\tau_{fast}$ | $\tau_{slow}$ | Percent fast | Percent slow | $\tau$ | $\tau^*$ |
| | *ms* | *ms* | | | | |
| 4D0709 | 2.09 | 5.94 | 39 | 61 | 5.09 | 4.39 |
| 51102230 | 1.37 | 10.48 | 78 | 22 | 14.51 | 15.20 |
| 51101821 | 2.57 | 11.03 | 40 | 60 | 13.79 | 13.79 |
| 5314014 | 0.98 | 10.41 | 20 | 80 | 8.38 | 6.49 |
| 511108 | 1.89 | 6.86 | 53 | 47 | 2.84 | 2.23 |
| mean | 1.8 | 8.9 | 46 | 54 | 8.9 | 8.42 |
| ±SEM | 0.3 | 1.1 | 10 | 10 | 2.3 | 2.6 |

Ensemble average tail currents average steps to −20 mV were fit by one exponential. $\tau^*$ values are from exponential fits of reopening-free ensemble average tail currents.

activates at more negative potentials than the fast component. Indeed, after depolarizations to −20 mV, macroscopic tail currents consist mainly of the slow component, with little or no detectable fast component. We wished to test whether individual L-channels could reproduce this macroscopic behavior. Therefore, we recorded from single-channel patches using a depolarization protocol that allowed the simultaneous collection of tail openings after depolarizations to +50 and −20 mV (Fig. 6 *A*). Fig. 6 shows individual traces and the ensemble average traces (with overlaid exponential fits) from one of five single-channel patches that yielded double-exponential ensemble average tail currents in response to the +50-mV step. Table IV summarizes the data from all five single-channel patches. For ensemble average tails recorded after step depolarizations to +50 mV, the average values of the parameters $\tau_{fast}$, $\tau_{slow}$, and percent contribution to the total tail current for each component are not significantly different from whole-cell values ($P \geq 0.05$ in all cases). Ensemble average tails recorded after step depolarizations to −20 mV were monoexponential, with an average value for the time constant of tail current decay that is not significantly different from the whole-cell slow component. Thus, it appears that the macroscopic property of different voltage dependences of activation of the two components is also reflected in the gating behavior of individual L-channels.

The change from slow component monoexponential to biexponential deactivation with increasing depolarizations could be due to the following: (*a*) a voltage-dependent change in access to the two open states (i.e., where the slow open state is accessed at more negative potentials than the fast open state); or (*b*) a voltage-dependent change in reopening frequency (i.e., reflecting a gating process whereby reopenings are favored by smaller depolarizations). To distinguish between these two possibilities, we constructed reopening-free ensemble average tail currents from the tail traces recorded after the depolarization to −20 mV. The time constants of these ensemble averages are shown in Table IV (in the column labeled $\tau^*$). The average value for the reopening-free time constant is not significantly different from the whole-cell slow component ($P > 0.05$). Thus, changes in reopening frequency do not account for the voltage dependence of deactivation kinetics. Rather, the two open states are accessed with different voltage dependences: The slow open state is accessed at more negative potentials than the fast open state.

### *Single L-Channels Can Access Two Open States during Depolarizations*

Tail current openings that are evident upon repolarization reflect open states that are accessed during step depolarizations. Therefore, $GH_3$ cell L-channels that produce double-exponential ensemble average tail currents should have access to two open states during step depolarizations. To characterize these open states, we recorded events from single-channel patches during long (100-ms) depolarizations to +20 mV. At this potential, both components of whole-cell tail current (and presumably both open states) will be activated (Fass and Levitan, 1996). A representative open-time histogram is shown in Fig. 7. Two exponentials were re-

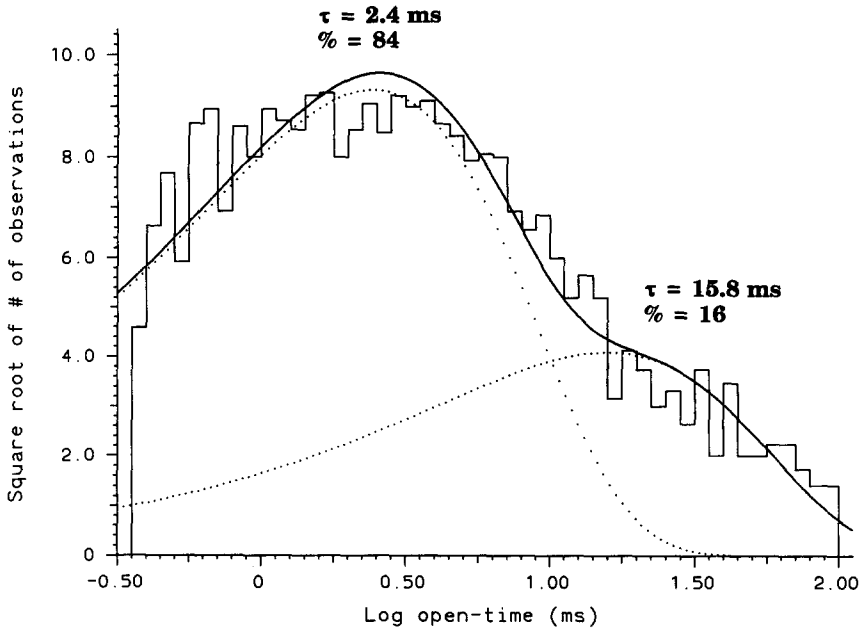


FIGURE 7. L-channel open times during depolarizations. Open-time data recorded during 100-ms depolarizations to +20 mV given to a single-channel patch are fit by two exponentials (see figure for time constants and percent values; percent values represent the portion of the area under the curve accounted for by each exponential component).

TABLE V

*Long Depolarizations Slow L-Channel Deactivation: Summary of Exponential Fits of Ensemble Average Tail Currents from Six Single-Channel Patches Subjected to 100-ms Depolarizations to +20 mV*

| Patch | $\tau_{fast}$ | $\tau_{slow}$ | Percent fast | Percent slow |
|---|---|---|---|---|
| | *ms* | *ms* | | |
| 5214010 | 1.1 | — | 100 | — |
| 52071430 | — | 15.9 | — | 100 |
| 513008 | — | 17.1 | — | 100 |
| 5117120 | 1.9 | 8.1 | 42 | 58 |
| 5207013 | 0.9 | 31.5 | 86 | 14 |
| 5215011 | 1.6 | 15.6 | 26 | 74 |
| mean ± SEM | 1.4 ± 0.2 | 17.6 ± 3.8 | 51 ± 18 | 49 ± 18 |

quired ($P < 0.0001$ in all cases) to fit open time histograms from five single-channel patches. The mean short open time was 2.5 ± 0.4 ms, whereas the mean long open time was 15.3 ± 1.4 ms. Thus, L-channels can access two open states during depolarizations.

*Long Depolarizations Slow L-Channel Deactivation in the Presence of Bay K 8644*

In the experiments in which we recorded events during long depolarizations, we also recorded the tail events after repolarization to −50 mV. We used the tail traces to construct ensemble average tail currents. The results of exponential fitting of these ensemble average tail currents for six single-channel patches are summarized in Table V. These data indicate that the mean value for the slow time constant of ensemble average tail current decay after long depolarizations ($\tau_{slow}$ = ~18 ms) was significantly larger ($P = 0.02$, unpaired $t$ test) than after short depolarizations (data from Table II where $\tau_{slow}$ = ~8 ms). This comparison across different patches raised the possibility that long depolarizations might slow L-channel deactivation.

To examine this effect on the macroscopic level directly, we used whole-cell recording of isolated L-currents. Fig. 8 *A* shows representative whole-cell L-currents evoked by short (20-ms) and long (200-ms) depolarizations to +20 mV given 10 s apart. The tail currents from these two traces are overlaid in Fig. 8 *B*. Tail current decay is slower after the longer depolarization. This effect was observed in all ($n = 5$) cells subjected to short and long depolarizations and did not depend on the order in which the depolarizations were given. We used exponential fitting of tail currents to quantify deactivation after short and long depolarizations. Table VI gives the means of parameters taken from these fits. After the short (20-ms) depolarizations, tails were fit by two exponentials. After the long (200-ms) depolarizations, two of five tail currents were fit by one exponen-

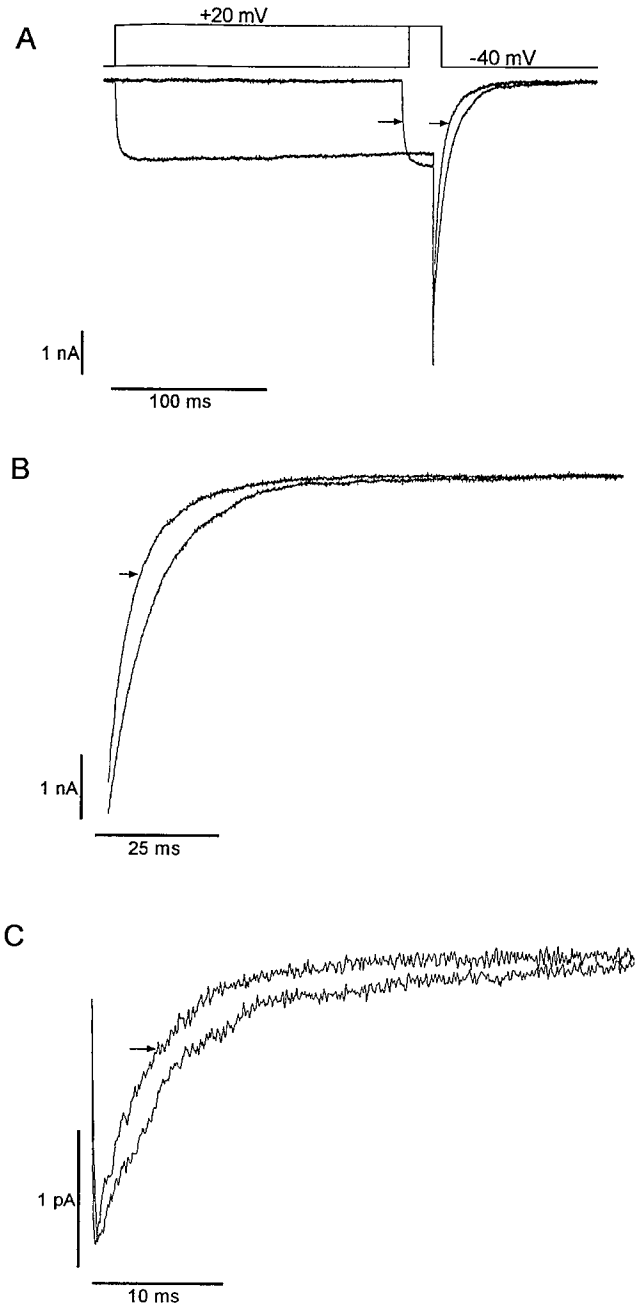


FIGURE 8. Whole-cell and single-channel ensemble average tail currents evoked by short and long depolarizations. (*A*) Whole-cell L-currents evoked by short (20-ms) and long (200-ms) depolarizations to +20 mV (voltage pulses are illustrated above traces). The two traces are aligned at the time of repolarization. Arrows indicate the current evoked by the short depolarization. (*B*) Whole-cell tail currents from the two traces in *A* are magnified in this panel. The arrow indicates the tail current after the short depolarization. (*C*) Ensemble average tail currents from a single-channel patch subjected to both short (20-ms) and long (100-ms) depolarizations to +20 mV. The plot shows only the portion of the traces recorded after the point of repolarization to −50 mV (note downward deflection reflecting repolarization). Short and long depolarizations were given at 0.5 Hz in alternating groups of 10 depolarizations. The arrow marks the ensemble average constructed from tail traces after the short depolarization.

TABLE VI

*Long Depolarizations Slow Deactivation of Whole-Cell L-Current: Means ($n = 5$) of Deactivation Parameters Taken from Exponential Fits of Tail Currents*

| Parameter | Short (20-ms) depolarizations | Long (200-ms) depolarizations |
|---|---|---|
| $\tau_{fast}$ | 1.96 ± 0.2 | 3.94 ± 0.3 |
| $\tau_{slow}$ | 7.67 ± 0.5 | 10.07 ± 0.4 |
| Percent fast | 36 ± 5.9 | 23 ± 6.8 |
| Percent slow | 64 ± 5.9 | 77 ± 6.8 |

Values are mean ± SEM.

tial with a time constant corresponding to the slow component of deactivation, whereas the other three tail currents were fit by two exponentials. The average time constants for both components are significantly larger ($P < 0.01$ in both cases) after the longer depolarization. The average proportion of the tail current made up by the fast component becomes significantly smaller, whereas the proportion made up by the slow component becomes significantly larger after the longer depolarization ($P < 0.05$ in both cases). These data imply that multiple changes in L-channel gating lead to a slowing of deactivation after long depolarizations.

For a direct comparison with the whole-cell data, we used a similar experimental protocol to record the effect of duration of depolarization on single L-channels. Fig. 8 *C* shows ensemble average tail currents constructed from traces taken from a single-channel patch subjected to both short (20-ms) and long (100-ms) depolarizations to +20 mV. In this and two other single-channel patches subjected to short and long depolarizations, ensemble average tail current decay is clearly slower after the long depolarization. The low number of events obtained in the individual patches (~60–200 events per ensemble average tail) precluded a curve-fitting analysis of the ensemble average tails or tail open-time histograms. For a rough quantitative comparison, we found the arithmetic means of tail open-times after short and long depolarizations: 2.1 ± 0.5 ms for tail events after short depolarizations; 3.1 ± 0.7 ms for tail events after long depolarizations (data from all three single-channel patches were combined to obtain these means). In two of the three single-channel patches, tail open-time arithmetic means were significantly different ($P < 0.05$ in both cases) after short versus long depolarizations. Reopenings occur at the same frequency ($P > 0.05$) after short and long depolarizations (29.3 ± 3.5 and 31.3 ± 4.3% of traces with events contain reopenings after short and long depolarizations, respectively). Thus, these data show that, like macroscopic L-current, the deactivation of single L-channels proceeds more slowly after longer depolarizations.

## DISCUSSION

### *Single $GH_3$ Cell L-Channels Can Give Rise to Two Components of Macroscopic L-Currents*

We used cell-attached patch recordings from $GH_3$ cells to measure the behavior of individual L-type $Ca^{2+}$ channels in the presence of Bay K 8644. Our main purpose was to elucidate the single-channel basis of the two components of macroscopic L-current in $GH_3$ cells recorded in the presence of Bay K 8644 (Fass and Levitan, 1996). The two macroscopic components have distinct deactivation kinetics (i.e., tail current decay is biexponential). To find the relationship between individual L-channels and macroscopic deactivation, we compared ensemble average tail currents constructed from data taken from single L-channels with whole-cell tail currents. The data presented in Table II show that ensemble average tail current decay of single L-channels can be biexponential with time constants that are similar to those obtained from macroscopic tail currents. Thus, an individual L-channel can reproduce both components of macroscopic tail currents.

Two additional observations support the conclusion that a single population of L-channels underlies macroscopic L-current. First, the voltage dependence of activation of the two components of ensemble average tail current decay of single L-channels exactly mirrors the voltage dependence of activation of the two whole-cell components: The slow component of ensemble average tail current decay is activated at more negative potentials than the fast component (Fig. 6 and Table IV). Second, deactivation of both single L-channels and whole-cell currents (Fig. 8) is slower after long depolarizations than after brief depolarizations. These observations, which show that the behavior of individual L-channels is sufficient to reproduce two major kinetic properties of macroscopic L-currents, provide further support for the conclusion that a single population of L-channels underlies whole-cell L-currents.

Table II shows that we also observed monoexponential ensemble average tail currents from single L-channels. The monoexponential tail currents have time courses of decay similar to the whole-cell fast component. These data appear to indicate the presence of a second population of L-channels in $GH_3$ cells. However, a single population of L-channels could produce both mono- and biexponential ensemble average tail currents if L-channels do not have continuous access to all possible gating pathways. In this case, L-channels with access to only a subset of the total possible gating pathways would produce monoexponential ensemble average tail currents. If these periods of limited access have average lifetimes on the scale of our typical patch recording (10–70 min), then we would obtain both mono- and biexponential ensemble average tail cur-

rents. The data shown in Fig. 5 suggest that this scenario may be correct. The plots of the open times of single L-channels over the time of the recording session in Fig. 5, *C* and *D*, show that transitions between periods of mostly long open times to mostly short open times, or vice versa, do occur. These transitions may represent changes in the access of individual L-channels to different subsets of conformational states. Thus, since access to different L-channel gating pathways appears to vary over time, our data suggest that a single population of L-channels may account for two components of macroscopic L-currents in $GH_3$ cells.

*Single L-Channels Access Multiple Open States*

A goal of this study is to deduce the series of conformational states accessed by L-channels in $GH_3$ cells that allow them to produce complex macroscopic current kinetics in the presence of Bay K 8644. Our data show that L-channels access at least two open states. Evidence for two open states comes from ensemble average tail currents that were constructed from data from single-channel patches using only those traces that contain no reopenings (described in Fig. 4 and Tables III and IV). Conceivably, reopenings (two types are shown in Fig. 4) might underlie the slower component of biexponential tail current decay. However, even without the effect of reopenings, ensemble average tail currents are biexponential. Since deactivation from a single open state would produce monoexponential ensemble average decay in the absence of reopenings, these data indicate that L-channels must access two open states.

Our data also provide information about the voltage dependence of access to the two open states. We assayed deactivation of individual L-channels after both small (to −20 mV) and large (to +50 mV) depolarizations (see Fig. 6 and Table IV). Ensemble average tail current decay after the small depolarization contains only the slow component, whereas ensemble average tail current decay after the large depolarization contains both components. Reopening-free ensemble average tail currents from traces recorded after the small depolarization show that the open state accessed during the small depolarization is the slow open state (Table IV, column marked $\tau^*$). Thus, the slow open state is accessed at more negative potentials than the fast open state. It is likely that this property underlies the different voltage dependences of activation of the two components of macroscopic deactivation.

*Mechanism of the Slowing of Deactivation by Long Depolarizations*

We found that lengthening the duration of depolarization slows L-channel deactivation (Fig. 8). Since the arithmetic mean of tail open times is increased by longer depolarizations, this effect involves, at least in part, a change in the access to L-channel open states. Perhaps the longer of the two open states (identified in tails after short depolarizations) is accessed more frequently after long depolarizations. However, this change alone would not produce the observed increase in the slow time constant of deactivation. Another possibility is that long depolarizations might increase the frequency of reopenings. However, analysis of reopening-free ensemble average tails evoked by long (100-ms) depolarizations to +20 mV (data not shown) indicates that reopenings do not play a significant role ($P > 0.05$) in the slowing of the time course of deactivation (i.e., reopening-free tails are slowed to the same degree as ensemble average tails constructed from all traces). Furthermore, in single-channel patches subjected to both short and long depolarizations, reopening frequency does not depend on duration of depolarization. Thus, long depolarizations may slow macroscopic deactivation by promoting access to additional (i.e., third, fourth, etc.) open states.

*Conductance of Single L-Channels in $GH_3$ Cells in the Presence of Bay K 8644*

Two previous studies have addressed the issue of the conductance (with high concentrations of $Ba^{2+}$ as the charge carrier) of L-channels in $GH_3$ cells in the presence of dihydropyridine agonists (Kunze and Ritchie, 1990; Mantegazza et al., 1995). Kunze and Ritchie (1990) observed four conductance levels in the presence of Bay K 8644: 9, 12, 16, and 24 pS. The predominant conductance levels were 12 and 16 pS. Mantegazza et al. (1995) observed three conductance levels in the presence of (S) + 202–791: ~25, ~22, and ~20 pS. The vast majority of the openings were to the ~25-pS level, whereas openings to the two lower conductance states were much rarer. Our data are consistent with aspects of both studies. First, we observed rare low conductance openings, which may correspond to the 9-pS conductance level reported by Kunze and Ritchie (1990). Since we obtained some patches that contained only these very low conductance openings, we believe that they may arise from a separate population of channels in $GH_3$ cells. Second, we observed primarily ~24-pS openings, which likely correspond to the ~25-pS level reported by Mantegazza et al. (1995). Third, our amplitude histograms occasionally contained minor medium amplitude components, which may correspond to the subconductance levels reported by either group. Our results differ from those of Kunze and Ritchie (1990), while agreeing with those of Mantegazza et al. (1995), in that the vast majority of the openings we observed were to the ~24-pS conductance level. The difference between our data and those of Kunze and Ritchie (1990) may arise from the fact that we used cell-attached

patch recording exclusively, whereas they used both cell-attached and outside-out patch methods. It is likely that most L-channels in $GH_3$ cells open mainly to the ~24-pS conductance level, since the averaged behavior of patches containing single ~24-pS L-channels reproduces all whole-cell phenomena.

*Complexity of L-Channels in Clonal Pituitary $GH_3$ Cells*

In our previous study of $GH_3$ cells (Fass and Levitan, 1996), we identified two exponential components in Bay K 8644–modified macroscopic L-channel tail currents that are not evident in all cell types that express L-channels (Droogmans and Callewaert, 1986; Marks and Jones, 1992; Bechem and Hoffmann, 1993; Zidanic and Fuchs, 1995). Two hypothetical mechanisms may account for these two components: (*a*) two populations of physically distinct L-channels, with each population contributing one component to the macroscopic tail current; or (*b*) a single population of L-channels with complex gating kinetics that produces both components of the macroscopic tail current. In this study, we have found evidence in favor of the second mechanism. We have shown that the two exponential components of macroscopic Bay K 8644–modified L-channel tail current can be produced by a single population of L-channels that have access to multiple open states. Similarly, multiple components of macroscopic L-current in rat ventricular myocytes (Richard et al., 1990, 1993) cells are likely produced by a single population of L-channels. Also, evidence from single-channel recordings suggests that one type of L-channel in rat cerebellar granule cells can produce two different gating patterns (Forti and Pietrobon, 1993). Thus, the interpretation of complex L-current waveforms should include a consideration of the possibility that a single population of L-channels may produce multiple macroscopic components.

Bay K 8644–modified $GH_3$ L-channels use multiple open states. Two of these open states produce the two components of macroscopic tail currents observed after short depolarizations. Long depolarizations slow macroscopic tail current decay, seemingly by promoting access to additional open states. Thus, in addition to contributing multiple components to macroscopic currents, L-channels may access multiple open states within the gating scheme inherent to each component. There are numerous determinants of access to these multiple open states: voltage (at least two of the open states are accessed with different voltage dependences); length of depolarization (additional open states are accessed with longer depolarizations); and unknown factors (access to the various open states can differ substantially between individual L-channels and can change over time). The fact that thyrotropin-releasing hormone inhibits the slow macroscopic component to a greater degree than the fast component (Fass and Levitan, 1996) suggests that modulators may distinguish between L-channels that are accessing different sets of open states. Thus, it appears that L-channels in clonal pituitary $GH_3$ cells have an array of gating possibilities under the regulation of recent electrical and biochemical events.

Funding for this study was provided by a grant-in-aid from the American Heart Association (AHA, Pennsylvania affiliate), a Klingenstein Fellowship in the Neurosciences, and National Institutes of Health grants NS29804 and NS32385 to E.S. Levitan. D.M. Fass was supported by a National Institute of Mental Health training grant (MH18273) and by predoctoral fellowships from the AHA (Pennsylvania affiliate) and the Andrew Mellon Foundation. E.S. Levitan is an Established Investigator of the AHA.

*Original version received 8 December 1995 and accepted version received 3 April 1996.*

REFERENCES

Bechem, M., and M. Hoffmann. 1993. The molecular mode of action of the Ca agonist (−) Bay K 8644 on the cardiac Ca channel. *Pflüg. Arch. Eur. J. Physiol.* 424:343–353.

Droogmans, G., and G. Callewaert. 1986. $Ca^{2+}$-channel current and its modification by the dihydropyridine agonist Bay k 8644 in isolated smooth muscle cells. *Pflüg. Arch. Eur. J. Physiol.* 406:259–265.

Duchemin, A.M., J.A. Enyeart, B.A. Biagi, D.N. Foster, B. Mlinar, and J.J. Enyeart. 1992. $Ca^{2+}$ channel modulation and kinase-C activation in a pituitary cell line: induction of immediate early genes and inhibition of proliferation. *Mol. Endocrinol.* 6:563–571.

Enyeart, J.J., T. Aizawa, and P.M. Hinkle. 1985. Dihydropyridine $Ca^{2+}$ antagonists: potent inhibitors of secretion from normal and transformed pituitary cells. *Am. J. Physiol.* 248:C510–C519.

Fass, D.M., and E.S. Levitan. 1996. Bay K 8644 reveals two components of L-type $Ca^{2+}$ channel current in clonal rat pituitary cells. *J. Gen. Physiol.* 108:1–11.

Forti, L., and D. Pietrobon. 1993. Functional diversity of L-type calcium channels in rat cerebellar neurons. *Neuron.* 10:437–450.

Hamill, O.P., A. Marty, E. Neher, B. Sakmann, and F.J. Sigworth. 1981. Improved patch-clamp techniques for high-resolution current recording from cells and cell-free membrane patches. *Pflüg. Arch. Eur. J. Physiol.* 391:85–100.

Hess, P. 1990. Calcium channels in vertebrate cells. *Annu. Rev. Neurosci.* 13:337–356.

Hille, B. 1992. Ionic Channels of Excitable Membranes. 2nd ed. Sinauer Associates, Inc., Sunderland, MA. 607 pp.

Kunze, D.L., and A.K. Ritchie. 1990. Multiple conductance levels of the dihydropyridine-sensitive calcium channel in $GH_3$ cells. *J. Membr. Biol.* 118:171–178.

Levitan, E.S., and R.H. Kramer. 1990. Neuropeptide modulation of single calcium and potassium channels detected with a new patch clamp configuration. *Nature (Lond.).* 348:545–547.

Lievano, A., A. Bolden, and R. Horn. 1994. Calcium channels in ex-

citable cells: divergent genotypic and phenotypic expression of $\alpha_1$ subunits. *Am. J. Physiol.* 267:C411–C424.

Mantegazza, M., C. Fasolato, J. Hescheler, and D. Pietrobon. 1995. Stimulation of single L-type calcium channels in rat pituitary $GH_3$ cells by thyrotropin-releasing hormone. *EMBO (Eur. Mol. Biol. Organ.) J.* 14:1075–1083.

Marks, T.N., and S.W. Jones. 1992. Calcium currents in the A7r5 smooth muscle–derived cell line. *J. Gen. Physiol.* 99:367–390.

McDonald, T.F., S. Pelzer, W. Trautwein, and D.J. Pelzer. 1994. Regulation and modulation of calcium channels in cardiac, skeletal, and smooth muscle cells. *Physiol. Rev.* 74:365–507.

Mollard, P., J.-M. Theler, N. Guérineau, P. Vacher, C. Chiavaroli, and W. Schlegel. 1994. Cytosolic $Ca^{2+}$ of excitable pituitary cells at resting potentials is controlled by steady state $Ca^{2+}$ currents sensitive to dihydropyridines. *J. Biol. Chem.* 269:25158–25164.

Murphy, T.H., P.J. Worley, and J.M. Baraban. 1991. L-type voltage-sensitive calcium channels mediate synaptic activation of immediate early genes. *Neuron.* 7:625–635.

Richard, S., P. Charnet, and J.M. Nerbonne. 1993. Interconversion between distinct gating pathways of the high threshold calcium channel in rat ventricular myocytes. *J. Physiol. (Camb.).* 462:197–228.

Richard, S., F. Tiaho, P. Charnet, J. Nargeot, and J.M. Nerbonne. 1990. Two pathways for $Ca^{2+}$ channel gating differentially modulated by physiological stimuli. *Am. J. Physiol.* 258:H1872–H1881.

Scherübel, H., and J. Hescheler. 1991. Steady-state currents through voltage-dependent, dihydropyridine-sensitive $Ca^{2+}$ channels in $GH_3$ pituitary cells. *Proc. R. Soc. Lond. Ser. B Biol. Sci.* 245: 127–131.

Sigworth, F.J., and S.M. Sine. 1987. Data transformations for improved display and fitting of single-channel dwell time histograms. *Biophys. J.* 52:1047–1054.

Tanabe, T., B.A. Adams, S. Numa, and K.G. Beam. 1991. Repeat I of the dihydropyridine receptor is critical in determining calcium channel activation kinetics. *Nature (Lond.).* 352:800–803.

Tiaho, F., C. Piot, J. Nargeot, and S. Richard. 1994. Regulation of the frequency-dependent facilitation of L-type $Ca^{2+}$ currents in rat ventricular myocytes. *J. Physiol. (Camb.).* 477:237–252.

Zidanic, M., and P.A. Fuchs. 1995. Kinetic analysis of barium currents in chick cochlear hair cells. *Biophys. J.* 68:1323–1336.